PHYSICAL REVIEW E **80**, 010401(R) (2009)

Brownian vortexes

Bo Sun,[1] Jiayi Lin,[2] Ellis Darby,[2] Alexander Y. Grosberg,[1] and David G. Grier[1]
[1]*Department of Physics and Center for Soft Matter Research, New York University, New York, New York 10003, USA*
[2]*NEST+m, 111 Columbia Street, New York, New York 10002, USA*
(Received 15 March 2009; published 8 July 2009)

Mechanical equilibrium at zero temperature does not necessarily imply thermodynamic equilibrium at finite temperature for a particle confined by a static but nonconservative force field. Instead, the diffusing particle can enter into a steady state characterized by toroidal circulation in the probability flux, which we call a Brownian vortex. The circulatory bias in the particle's thermally driven trajectory is not simply a deterministic response to the solenoidal component of the force but rather reflects interplay between advection and diffusion in which thermal fluctuations extract work from the nonconservative force field. As an example of this previously unrecognized class of stochastic heat engines, we consider a colloidal sphere diffusing in a conventional optical tweezer. We demonstrate both theoretically and experimentally that nonconservative optical forces bias the particle's fluctuations into toroidal vortexes whose circulation can reverse direction with temperature or laser power.

DOI: 10.1103/PhysRevE.80.010401 PACS number(s): 82.70.Dd, 05.40.Jc, 05.60.Cd, 87.80.Cc

Stochastic heat engines such as thermal ratchets and Brownian motors use nonconservative forces to eke fluxes of energy or probability out of otherwise random thermal fluctuations [1]. In virtually all previous reports, such noise-driven machines have relied on a time-dependent force to rectify fluctuations. Here, we demonstrate that time-independent force fields can also create stochastic heat engines so long as the force has an irrotational component capable of confining the particle and a nonvanishing solenoidal component. The resulting interplay of advection and diffusion gives rise to toroidal probability currents that we refer to as the Brownian vortexes. As an illustration, we reinterpret the recently discovered circulation of a colloidal sphere in an optical tweezer [2] in light of this insight and demonstrate that it constitutes a practical realization of a Brownian vortex. One consequence is the prediction, which we confirm both through simulation and experimentally, that a trapped particle's circulation can undergo flux reversal with continuous changes in laser power or temperature. These observations reveal that flux reversal in the Brownian vortexes proceeds through a surprising and distinctive two-stage mechanism.

Our discussion focuses on a single particle's motions through a viscous medium that also acts as a thermodynamic heat bath at temperature T. The particle moves under the influence of a static force field,

$$\boldsymbol{F}(\boldsymbol{r}) = -\nabla U + \nabla \times \boldsymbol{A}, \tag{1}$$

that is factored uniquely into a conservative irrotational component described by the scalar potential $U(\boldsymbol{r})$ and a nonconservative solenoidal component derived from the vector potential $\boldsymbol{A}(\boldsymbol{r})$. We assume that $\boldsymbol{F}(\boldsymbol{r})$ has at least one point of stable mechanical equilibrium so that the particle does not move at $T=0$. This distinguishes the system from a deterministic machine that is merely advected by a nonconservative force.

Thermal fluctuations enable the particle to explore the force landscape, and we further assume that $\boldsymbol{F}(\boldsymbol{r})$ confines the particle so that its probability density $\rho(\boldsymbol{r})$ does not change with time. The probability flux,

$$\boldsymbol{j}(\boldsymbol{r}) = \mu\rho(\boldsymbol{r})\boldsymbol{F}(\boldsymbol{r}) - \mu k_B T \nabla \rho(\boldsymbol{r}), \tag{2}$$

reflects both the particle's response to the force field through its mobility, μ, and also its diffusivity at temperature T. Because there are no sources or sinks of probability, $\nabla \cdot \boldsymbol{j} = \boldsymbol{0}$, and the flux either vanishes in equilibrium ($\nabla \times \boldsymbol{A} = \boldsymbol{0}$) or else forms closed loops in steady state ($\nabla \times \boldsymbol{A} \neq \boldsymbol{0}$). Circulation around these loops is measured by

$$\nabla \times \boldsymbol{j} = \mu\rho\boldsymbol{\omega} + \mu \nabla \rho \times \boldsymbol{F}, \tag{3}$$

where $\boldsymbol{\omega}(\boldsymbol{r}) = -\nabla^2 \boldsymbol{A}$ is the vorticity in $\boldsymbol{F}(\boldsymbol{r})$ [3]. Vortexes can form in $\boldsymbol{j}(\boldsymbol{r})$ even if $\boldsymbol{F}(\boldsymbol{r})$ does not have closed loops because the diffusive flux represented by the second term in Eq. (3) provides the return flow.

Both the magnitude and the direction of $\boldsymbol{\omega}(\boldsymbol{r})$ can vary with position. The rate and direction of the particle's circulation therefore depend on the domain over which the particle can diffuse at temperature T. Changing the temperature changes this range and therefore can reverse the sense of the overall circulation. The possibility of temperature-dependent flux reversal distinguishes the Brownian vortex circulation from the more familiar interplay of advection and diffusion in such systems as the electric current flowing through a battery-powered circuit.

As a concrete example, we consider the motions of a colloidal sphere in an optical tweezer, a single-beam optical gradient force trap created with a strongly focused beam of light [4]. Recent three-dimensional particle-tracking measurements [2] have revealed a previously unsuspected toroidal bias in the trapped particle's diffusion, which is depicted schematically in Fig. 1(a). Whereas intensity gradients draw the particle to the beam's focus with a manifestly conservative restoring force, nonconservative radiation pressure biases its fluctuations [2]. This cannot constitute an example of a Brownian motor, as was suggested in Ref. [2], because Brownian motors rely on time-dependent forcing to break detailed balance [1]. A more detailed examination of the

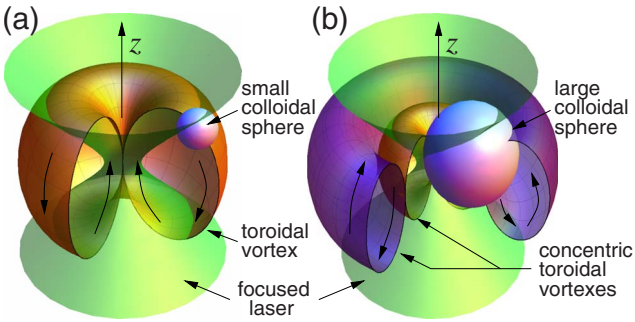

FIG. 1. (Color online) Schematic representation of a colloidal sphere undergoing toroidal circulation in an optical tweezer. (a) The Rayleigh limit, $a<\lambda$. (b) Larger spheres, $a>\lambda$.

forces acting on the trapped particle instead reveals this system's true nature as a Brownian vortex.

Figure 2(a) shows streamlines of the force field computed with Lorenz-Mie theory [5,6] for an 800-nm-diameter polystyrene sphere trapped by an optical tweezer in water. This is a fully vectorial treatment for a beam with vacuum wavelength of $\lambda=532$ nm propagating in the $\hat{z}$ direction and brought to a focus by an ideal lens with numerical aperture 1.4. Streamlines are projected into the (r,z) plane in cylindrical coordinates, $\boldsymbol{r}=(r,\phi,z)$. Figures 2(b) and 2(c) show the irrotational and solenoidal components of the force field, respectively, which were obtained through the Helmholtz-Hodge decomposition [3].

The particle's thermally driven trajectory $\boldsymbol{r}_p(t)$ through $\boldsymbol{F}(\boldsymbol{r})$ was computed with a Brownian dynamics simulation of the Langevin equation,

$$\dot{\boldsymbol{r}}_p = \mu\boldsymbol{F}(\boldsymbol{r}_p) + \mu\boldsymbol{f}(t), \tag{4}$$

where $\mu=(6\pi\eta a)^{-1}$ is the Stokes mobility for a sphere of radius a moving through a fluid of viscosity η and where the stochastic force due to thermal fluctuations satisfies $\langle\boldsymbol{f}(t)\rangle=0$ and $\langle\boldsymbol{f}(t)\cdot\boldsymbol{f}(t')\rangle=2\mu^{-1}k_BT\delta(t-t')$. The probability distribution and flux then are computed with nonparametric density estimators [7] as

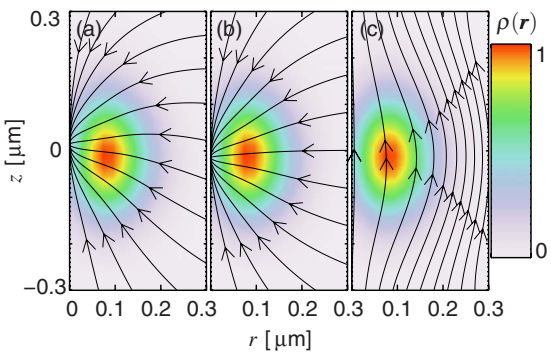

FIG. 2. (Color online) (a) Streamlines of the computed optical force calculated as tangent curves to $\boldsymbol{F}(\boldsymbol{r})$ in the (r,z) plane. This representation indicates the force's direction but not its magnitude. Background images show $\rho(\boldsymbol{r})$ at $T=21$ °C and a laser power of 0.3 W. (b) Streamlines of the irrotational component of the force, $-\nabla U$. (c) Streamlines of the solenoidal component of the force, $\nabla\times\boldsymbol{A}$.

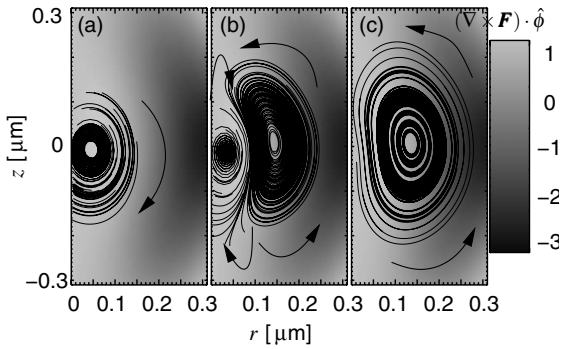

FIG. 3. Streamlines of the simulated probability flux for a sphere diffusing in the optical force field of Fig. 2. (a) Forward circulation at $P=0.7$ W. (b) Counter-rotating vortexes at $P=0.5$ W. (c) Complete flux reversal at $P=0.3$ W. Images show the normalized vorticity of $\boldsymbol{F}(\boldsymbol{r})$.

$$\rho(\boldsymbol{r}) = \frac{1}{(2\pi\sigma)^{3/2}}\left\langle \exp\left(-\frac{|\boldsymbol{r}-\boldsymbol{r}_p(t)|^2}{2\sigma^2}\right)\right\rangle \tag{5}$$

and

$$\boldsymbol{j}(\boldsymbol{r}) = \frac{1}{(2\pi\sigma)^{3/2}}\left\langle \boldsymbol{r}_p(t)\exp\left(-\frac{|\boldsymbol{r}-\boldsymbol{r}_p(t)|^2}{2\sigma^2}\right)\right\rangle, \tag{6}$$

where σ is chosen to minimize the variance in $\rho(\boldsymbol{r})$ without unnecessary blurring.

Shading in Fig. 2 represents $\rho(\boldsymbol{r})$ at $T=21$ °C for an optical tweezer powered by $P=0.3$ W. Neither $\boldsymbol{F}(\boldsymbol{r})$ nor its solenoidal component display loops in the range of the particle's diffusion. Nevertheless, streamlines of $\boldsymbol{j}(\boldsymbol{r})$ plotted in Fig. 3 show loops in the (r,z) plane consistent with the appearance of a toroidal vortex centered on the optical axis. It should be emphasized that the observed circulation is apparent only in a very long trajectory or in an ensemble average of shorter trajectories; the particle's short-time motion resembles a random walk in a harmonic well, its toroidal bias too subtle to be perceived.

Figure 3(a) shows streamlines at a comparatively large laser power, $P=0.7$ W, for which the particle is well localized near the optical axis. Under these conditions, the particle circulates in a single toroidal vortex, much as was predicted in Ref. [2] and portrayed in Fig. 1(a). The local circulation rate, $[\nabla\times\boldsymbol{j}(\boldsymbol{r})]\cdot\hat{\phi}$, is uniformly positive.

Reducing the laser power does not change the structure of the force field but reduces its overall magnitude. This is equivalent, therefore, to increasing the effective temperature. Doing so increases the range over which the particle can wander and enables it to populate a second concentric counter-rotating vortex, as plotted in Fig. 3(b) for $P=0.5$ W, and indicated schematically in Fig. 1(b).

At still lower laser power (or higher temperature), the outer vortex subsumes the inner vortex, and the probability current circulates once again in a single toroidal roll but with its direction reversed. Complete flux reversal is demonstrated in Fig. 3(c) for $P=0.3$ W.

Such two-stage flux reversal is not observed in the Brownian motors or related temporally driven stochastic heat

engines. Its origin can be found in the vorticity of the force field in Fig. 3. Although the solenoidal component of the optical force, $\nabla \times \boldsymbol{A}$, is directed uniformly upward, its curl, $\nabla \times \boldsymbol{F}$, changes direction with distance from the optical axis. So long as the particle's probability density is concentrated in regions where $\omega(\boldsymbol{r}) \cdot \hat{\phi}$ is positive, as is the case in Fig. 3(a), the overall circulation of the probability flux also is positive. When the particle wanders into regions of negative vorticity, it circulates in the retrograde direction, as shown in Fig. 3(b). In both cases, the nonconservative part of the optical force field redistributes $\rho(\boldsymbol{r})$ downstream of the beam's focal point and diffusion provides the return current. The single-roll structure reasserts itself in the flux-reversed state when gradients in $\rho(\boldsymbol{r})$ become large enough for diffusion to outstrip advection along the optical axis.

We also observed flux reversal in Brownian vortex circulation through experimental observations of colloidal spheres trapped in optical tweezers. Our system consists of 1.5 μm diameter colloidal silica spheres (Bangs Laboratories, Lot SS04N/5252) dispersed in a 50-μm-thick layer of water that is hermetically sealed between a clean glass slide and a No. 1.5 cover slip. The sample is mounted on the stage of an inverted light microscope (Nikon TE 2000U) where it is observed with a 100× numerical aperture 1.4 oil immersion objective lens (Nikon Plan Apo). The same objective lens is used to focus four holographic optical tweezers [8–11] arranged at the corner of a square with 30 μm sides near the midplane of the sample. These traps are powered by a single laser (Coherent Verdi 5W, $\lambda = 532$ nm) that is imprinted with a computer-generated hologram [10] by a liquid-crystal spatial light modulator (Hamamatsu X7665-16) before being projected into the sample. The trap array is designed so that two of the traps have nearly the same intensity, the third is slightly brighter, and the fourth is brighter still. This enables us to seek out intensity-dependent differences in simultaneously acquired data sets and thus to avoid artifacts due to vibrations or other instrumental fluctuations.

The trapped spheres' three-dimensional motions are measured with nanometer resolution through quantitative analysis [12] of images obtained with holographic video microscopy [13,14]. Holographic images are obtained by illuminating the sample with the collimated beam from a HeNe laser (Uniphase 10 mW) operating at 632.8 nm. Light scattered by the particles interferes with the unscattered portion of the beam in the microscope's focal plane to create an in-line hologram that is magnified and recorded by a video camera (NEC TI-324AII) at 30 frames/s. Radiation pressure due to the nW/μm^2 intensity of the imaging beam is negligible compared with thermal forces and forces due to the optical trap and so does not affect the particles' trajectories.

Both fields of each interlaced holographic video frame were analyzed with Lorenz-Mie light-scattering theory [5,12] to measure each sphere's three-dimensional position $\boldsymbol{r}(t)$, with 3 nm in-plane resolution and 10 nm axial resolution [12]. A total of 32-min-long trajectories were acquired at constant laser power for the four particles. At the end of each acquisition period, the trapped particles were moved automatically out of the field of view to acquire background holograms and to confirm the system's stability. Each particle's trajectories were analyzed with Eqs. (5) and (6) to visualize the mean circulation and the results combined into maps of the mean circulation for each trap. In all, more than 100 000 holograms were analyzed for each trap.

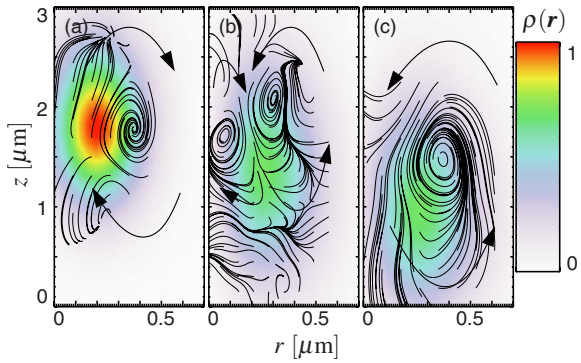

FIG. 4. (Color online) Streamlines of the measured circulation of optically trapped silica spheres. (a) $k_\perp = 6.56$ pN/μm: single positive toroidal roll. (b) $k_\perp = 2.43$ pN/μm: concentric counter-rotating rolls. (c) $k_\perp = 2.27$ pN/μm: flux reversal. Single retrograde roll. Background images show measurements of $\rho(\boldsymbol{r})$ for each set of conditions.

Figure 4 shows streamlines of the trajectories for three of the four particles, the fourth serving as a control for Fig. 4(c). These results confirm not only the presence of toroidal circulation in the particles' motions but also the appearance of flux reversal as a function of trap strength. Each trap-particle combination is characterized by its apparent [2] in-plane stiffness, $k_\perp$, which is obtained from statistical analysis of the particle's measured in-plane fluctuations [10], stiffer traps corresponding to higher laser power and lower effective temperature. The traps' apparent axial stiffness is a factor of 5 smaller than their lateral stiffness because axial intensity gradients are correspondingly weaker [2,15].

The stiffest trap, shown in Fig. 4(a), concentrates its particle's probability density $\rho(\boldsymbol{r})$ closest to the optical axis and displays a single roll circulating in the positive sense. The weaker trap in Fig. 4(b) allows the trapped particle to wander further afield, where it enters into concentric counter-rotating rolls, similar to the simulated results in Fig. 3(b). The weakest traps, one of which is represented in Fig. 4(c), both display a single retrograde roll in $\boldsymbol{j}(\boldsymbol{r})$ and thus demonstrate complete flux reversal.

The probability distribution is centered lower in the weaker traps because of gravity acting on the silica spheres, whose 1.9 g/cm^3 density exceeds that of the surrounding water. This additional conservative force does not directly contribute to the particles' circulation but does affect what region of the optical force field the particle occupies for a given laser power. Undoubtedly, this influenced the trend in Fig. 4 but does not change our interpretation of the phenomenon as two-stage flux reversal in a Brownian vortex.

Instrumental fluctuations cannot account for our observations because all four measurements were performed simultaneously in a static array of optical traps derived from the same laser beam. The particles are sufficiently separated from each other and from the walls of their container that hydrodynamic coupling also is unlikely to have influenced their motion [16]. Rather, the Brownian vortex circulation,

including power-dependent flux reversal, appears to be an inherent aspect of the statistics of colloidal spheres in optical tweezers.

In this Rapid Communication, we have introduced the Brownian vortex as a distinct class of noise-driven machines. Unlike stochastic heat engines driven by time-dependent forces [1], the Brownian vortexes arise in static force fields possessing both potential and nonconservative solenoidal components. Because one-dimensional force fields have no solenoidal component, the Brownian vortex has no one-dimensional manifestation. Not any static force field, furthermore, can support a Brownian vortex. For example, a force field lacking a sufficiently strong confining potential cannot establish the requisite probability-conserving steady state. Still other force fields establish circulating steady states without thermal noise. An example of this is provided by the ringlike optical trap known as an optical vortex [17] that exerts torques on trapped objects [18] through its helical wave-front structure [19]. These are deterministic machines rather than stochastic heat engines and so are not the Brownian vortexes.

Although the simulations and experiments presented here focus on colloidal circulation in optical tweezers, the Brownian vortex is a general phenomenon. Seeking its signature in such contexts as biological networks and financial systems, as well as in new mechanical models, should provide opportunities for future research. Further work also is required to elucidate Brownian vortexes' thermodynamic properties, particularly the considerations that determine their thermodynamic efficiency.

We acknowledge fruitful conversations with Yohai Roichman. This work was supported by the MRSEC program of the NSF under Grant No. DMR-0820341. B.S. acknowledges support from the Kessler Family Foundation.

[1] P. Reimann, R. Bartussek, R. Haussler, and P. Hänggi, Phys. Lett. A **215**, 26 (1996); H. Linke, Appl. Phys. A **75**, 167 (2002); R. D. Astumian and P. Hänggi, Phys. Today **55** (11), 33 (2002); P. Reimann, Phys. Rep. **361**, 57 (2002); P. Reimann and P. Hänggi, Appl. Phys. A **75**, 169 (2002).

[2] Y. Roichman, B. Sun, A. Stolarski, and D. G. Grier, Phys. Rev. Lett. **101**, 128301 (2008).

[3] L. Morino, Comput. Mech. **1**, 65 (1986).

[4] A. Ashkin, J. M. Dziedzic, J. E. Bjorkholm, and S. Chu, Opt. Lett. **11**, 288 (1986).

[5] C. F. Bohren and D. R. Huffman, *Absorption and Scattering of Light by Small Particles* (Wiley Interscience, New York, 1983).

[6] B. Sun, Y. Roichman, and D. G. Grier, Opt. Express **16**, 15765 (2008).

[7] B. W. Sliverman, *Density Estimation for Statistics and Data Analysis* (Chapman & Hall, New York, 1992).

[8] E. R. Dufresne and D. G. Grier, Rev. Sci. Instrum. **69**, 1974 (1998).

[9] D. G. Grier, Nature (London) **424**, 810 (2003).

[10] M. Polin, K. Ladavac, S.-H. Lee, Y. Roichman, and D. G. Grier, Opt. Express **13**, 5831 (2005).

[11] Y. Roichman, A. S. Waldron, E. Gardel, and D. G. Grier, Appl. Opt. **45**, 3425 (2006).

[12] S.-H. Lee, Y. Roichman, G.-R. Yi, S.-H. Kim, S.-M. Yang, A. van Blaaderen, P. van Oostrum, and D. G. Grier, Opt. Express **15**, 18275 (2007).

[13] J. Sheng, E. Malkiel, and J. Katz, Appl. Opt. **45**, 3893 (2006).

[14] S.-H. Lee and D. G. Grier, Opt. Express **15**, 1505 (2007).

[15] K. C. Vermeulen, G. J. L. Wuite, G. J. M. Stienen, and C. F. Schmidt, Appl. Opt. **45**, 1812 (2006).

[16] J. C. Crocker, J. Chem. Phys. **106**, 2837 (1997); E. R. Dufresne, T. M. Squires, M. P. Brenner, and D. G. Grier, Phys. Rev. Lett. **85**, 3317 (2000); E. R. Dufresne, D. Altman, and D. G. Grier, Europhys. Lett. **53**, 264 (2001); M. Polin, D. G. Grier, and S. R. Quake, Phys. Rev. Lett. **96**, 088101 (2006).

[17] H. He, N. R. Heckenberg, and H. Rubinsztein-Dunlop, J. Mod. Opt. **42**, 217 (1995); N. B. Simpson, L. Allen, and M. J. Padgett, *ibid.* **43**, 2485 (1996); K. T. Gahagan and G. A. Swartzlander, Opt. Lett. **21**, 827 (1996).

[18] H. He, M. E. J. Friese, N. R. Heckenberg, and H. Rubinsztein-Dunlop, Phys. Rev. Lett. **75**, 826 (1995).

[19] L. Allen, M. W. Beijersbergen, R. J. C. Spreeuw, and J. P. Woerdman, Phys. Rev. A **45**, 8185 (1992); Y. Roichman, B. Sun, Y. Roichman, J. Amato-Grill, and D. G. Grier, Phys. Rev. Lett. **100**, 013602 (2008).